Progress In Electromagnetics Research B, Vol. 54, 321–336, 2013

STAND-OFF DISTANCES FOR NON-LINE-OF-SIGHT MARITIME MOBILE APPLICATIONS IN 5 GHz BAND

Yee Hui Lee[1], Feng Dong[1], and Yu Song Meng[2, *]

[1]School of Electrical and Electronic Engineering, Nanyang Technological University, 50 Nanyang Avenue, Singapore 639798, Singapore

[2]National Metrology Centre, A*STAR (Agency for Science, Technology and Research), 1 Science Park Drive, Singapore 118221, Singapore

Abstract—Non-line-of-sight (NLoS) maritime mobile radio channel in 5 GHz band is experimentally investigated in this paper through wideband channel soundings. During the measurements, the transmitter was installed onboard a speed boat, while the receiver was placed on the roof top of a building on shore. Different types of cargo ships anchored off the east coast of Singapore were examined as obstructions for the NLoS propagations. Besides power delay profile (PDP), *stand-off distance* is introduced in this work to analyze the NLoS propagations associated with three different types of cargo ships. The measured PDPs and stand-off distances are found to be comparable qualitatively with the simulated results using 3-D ray tracing. The reported information is found to be useful for military applications such as unmanned surface vehicles (USVs) in maritime environments or surveillance.

1. INTRODUCTION

Radio-wave propagations in maritime environments have been the focus of much theoretical and experimental research over the years for different application scenarios [1–8]. From these literatures that address the characterizations of radio-wave behavior in maritime environments, some studies deal with the effect of evaporation duct [1, 2, 8], while others deal with the modeling and measurements for over-sea mobile radio channel at various frequencies [3–7].

Received 8 August 2013, Accepted 16 September 2013, Scheduled 16 September 2013

* Corresponding author: Yu Song Meng (ysmeng@ieee.org).

Recently, there has been a growing interest in the implementation of mobile radio system in the 5 GHz band [9–12]. As compared to the lower frequency (< 2 GHz) applications in [3, 4], high-speed or high-capacity wireless applications can be achieved at 5 GHz. For example, high-speed WiMAX at 5.8 GHz was studied in [9], and microwave landing system at 5 GHz was examined in [11, 12]. It has been shown that the 5 GHz band has a good potential for military applications [13], such as off-shore anti-terrorist surveillance or application of unmanned surface vehicles (USVs) in the maritime environment.

In general, these military applications operate in a near sea-surface line-of-sight (LoS) mobile environment (e.g., between a control station and a moving vessel). However for some maritime environments such as around the coast of the sea port island of Singapore, large vessels (e.g., cargo ships) crowd the coast lines. In such scenarios, the non-line-of-sight (NLoS) propagations created by the large vessels are often encountered. The large vessels are normally anchored about 3 km to 5 km off the shores. The study of NLoS propagation therefore becomes crucial since the 5 GHz microwave link can be shadowed/diffracted by the large metallic body of the vessels [14] anchored between the on-shore control station and the moving vessel. This makes the mobile radio channel challenging as compared to those reported in [4–7, 9], where most of the research works focus on the investigations of LoS radio-wave propagations in maritime environments. The NLoS propagations over the maritime environments are also different from those in urban areas [15, 16] and forested areas [17, 18] since the blockage in the maritime environment is caused by large metallic bodies. Therefore, it is of great interest and importance to investigate the NLoS maritime mobile radio channel in the 5 GHz band experimentally.

Because of the fact that the large metallic body of a cargo ship could fully block the propagation path and make the communication link almost impossible when a mobile vessel (e.g., an USV) is behind the cargo ship, a parameter *stand-off distance* is introduced in this paper. It is a parameter commonly used as in security and surveillance applications, and defines the minimum distance between a secured building or vehicle to any unauthorized intruders or a surveillance vehicle [19]. In this work given the fact that it deals with maritime surveillance applications, the stand-off distance is defined as the shortest distance at which an USV can approach a cargo ship, yet still be able to establish a reliable communication link with the control station on shore, when the cargo ship is in between the shore to sea communication path and acts as the obstruction ship as shown in Fig. 1. In this work, the stand-off distance is determined at the first

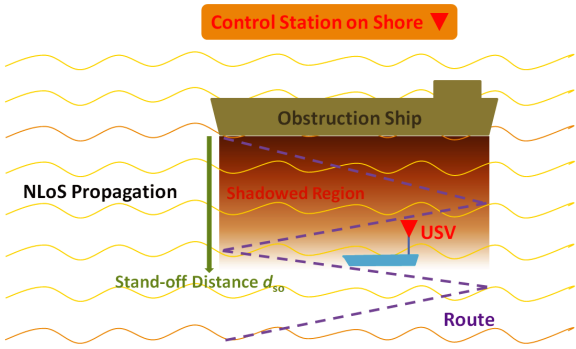

Figure 1. Positions for transmitter (USV) and receiver (control station), and measurement route.

local maximum point of the signal to noise ratio (SNR) value (larger than 10 dB) as the distance behind the obstruction ship increases.

In this paper as a continuation of previous work [20, 21], the shadowing/diffraction of a 5.5 GHz maritime mobile radio channel obstructed by different types of cargo ships is examined in details. The used channel sounding technique and the measurement setup are discussed in Section 2 where a brief description of the measurement plan is also given. In Section 3, performance comparisons between the ray tracing simulations and the measurement results are conducted. This is followed by the investigations of stand-off distance for different types of obstruction ships in Section 4. Finally, Section 5 gives a summary of the analyses performed in this paper.

2. MEASUREMENT CAMPAIGN

2.1. Channel Sounding and Measurement Setup

The spread-spectrum technique with the use of *maximal-length pseudonoise (PN) sequence* was implemented for channel sounding at the transmitter as in [7, 11, 12, 18]. In our measurements, a 1023-bit PN sequence with a dynamic range of 60.2 dB [22] was transmitted at a rate of 20 Mchips/s and modulated using Binary Phase Shift Key. This allows for a delay resolution of 50 ns for the measurements. For practical channel soundings, an omni-directional antenna with a gain of 9 dBi was mounted on top of a speed boat as shown in Fig. 2(a), at a height of approximately 3.5 m above the sea level. The antenna was connected to a vector signal generator through a high power amplifier (housed within the boat cabin), forming a mobile transmitter with its

(a) Transmitter on boat

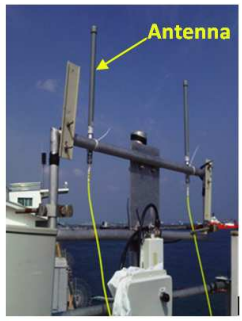

(b) Receiver on shore

(c) Three classified types of the obstruction ships

Figure 2. Measurement setup and different types of obstruction ships.

output power kept at 30 dBm. During the measurement, GPS data were logged continuously in order to obtain the instantaneous time, altitude, longitude and latitude coordinates. A fluxgate compass was used to log the pitch and roll of the moving boat.

As shown in Fig. 2(b), an identical omni-directional antenna was used for the signal reception. The antenna was mounted on the roof of a building at a height of about 10 m above the sea surface level regardless of tidal-wave changes. The received signal was then down-converted to a 20 MHz intermediate-frequency signal, and sampled at a rate of 100 Msamples/s. All the data recorded was time-stamped with the GPS information in order to synchronize the received signal with the location, heading and orientation of the mobile transmitter. Both the transmitter and receiver were also equipped with weather stations to record the weather conditions such as ambient temperature, humidity and wind speed. It is noted that the performance of all the systems was checked before and after the sea trials.

2.2. Measurement Plan

Measurements were carried out at the southeast coast of Singapore, where many large cargo ships were anchored about 3 km to 5 km off the shores. These cargo ships can generally be classified into three basic types as shown in Fig. 2(c); Type A ships are characterized by their low height above the sea level and their flat top structure; Type B

ships are also characterized by their low height above the sea level but having a complex periodic structure on its top, and Type C ships are characterized by their high height above the sea level and their flat top structure. The reason for the choice of such a measurement plan (i.e., the transmission range and transceiver heights) is due to the maritime surveillance applications under consideration; a 2-way communication link between an USV and a control station which is either on land or on a mother-ship is to be established [13]. During these scenarios, there is no LoS transmission. The cargo ships (obstruction ship) blocked the microwave link as shown in Fig. 1.

During the measurements, the boat carrying the transmitter went behind the obstruction ship to form an NLoS link as shown in Fig. 1. The control station was located at the coast right next to the shoreline. The maximum distance between the receiver (Rx) and the transmitter (Tx) was about 8 km with the obstruction ship at a maximum distance of 5 km away from the shore. The main focus of the study was to find the stand-off distances for the NLoS maritime surveillance applications in the 5 GHz band. The targeted obstruction ship type was chosen at the beginning of each trial. The measurements were conducted both in front of the ship (LoS) and behind the ship (NLoS) repeatedly. In the cases when the transmitting boat was hidden behind the obstruction ship, experimental data was continuously recorded while the boat moved away from the obstruction ship as shown in the measurement route of Fig. 1. The zigzag route was chosen as it could provide more information than a straight/circular route, and is also easier to be practically implemented using a speed boat in the sea.

In this study, the dimensions and structure of each obstruction ship are important variables that can influence the measurement results, and were obtained from the internet database using their International Maritime Organization number. More than 7 campaigns were conducted with 12 different cargo ships over a period of 3 months.

3. RAY TRACING AND VERIFICATIONS

3.1. Simulations Using Ray Tracing

Due to the nature of sea measurements which requires heavy logistics and manpower (is also time-consuming), ray tracing simulation is an alternative technique for understanding the shadowing/diffraction effects from three different types of obstruction ships. A ray tracing software, Wireless InSite [23], is used to model the maritime environment with a cargo ship as the obstruction ship. Simplified models for the transmitter boat used for simulation is shown in Fig. 3(a), the on-shore receiver is shown in Fig. 3(b), and the three

(a) Transmitter on boat

(b) Receiver on shore

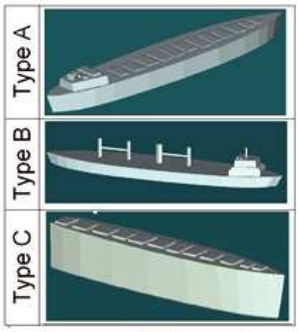

(c) Three types of obstruction ships

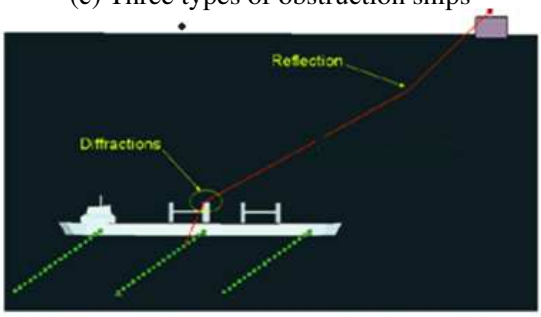

(d) Example of the simulation scenarios with a Type B obstruction ship

Figure 3. Simulation models in wireless InSite.

different types of obstruction ships are shown in Fig. 3(c). These models were drawn using the AutoCAD and imported into the Wireless InSite software for simulation purposes.

The parameters of the models including dimensions, material and shape, are all based on the actual values to the best of our knowledge. The 3-D model of the experiment scenario is then simulated to study the effects of transmission, reflection and diffraction using the ray tracing technique. The simulation was performed using a hybrid of the shooting bouncing ray (SBR) algorithm and the uniform theory of diffraction (UTD) [24]. The SBR technique is used to find the

propagation paths between the transmitter and the receiver. Once these propagation paths are determined, the UTD is implemented to evaluate the electric field for each path. One of the simulation scenarios where the transmitted signal from the boat undergoes the diffraction by the periodic structure on a Type B ship and then the reflection off the sea surface before arriving at the control station on land is shown in Fig. 3(d). Comparisons between the measurements and the simulation results are performed in the following subsection.

3.2. Verifications of Propagation Channels

The maritime mobile propagation channel can be modeled as a linear time-variant system, whose complex baseband equivalent channel impulse response $h(t,\tau)$ can be expressed as [7, 18],

$$h(t,\tau) = \sum_{k=0}^{N} a_k(t) \exp\{j\varphi_k(t)\}\delta\{\tau - \tau_k(t)\} \tag{1}$$

where t and τ are the observation and relative times of the impulse respectively, and $(t-\tau)$ is the application time. a_k, τ_k, and φ_k are the time-varying amplitude, propagation delay and phase shift of the kth delay tap which may consist of more than one multipath component due to the limitation of delay resolution (50 ns in this study). N is the number of delay taps of the channel of interest.

In this study, the empirical channel impulse response $\hat{h}(t,\tau)$ of the NLoS channel at 5.5 GHz was obtained by correlating the known transmitted signal with the received signal [7, 18, 22]. To evaluate

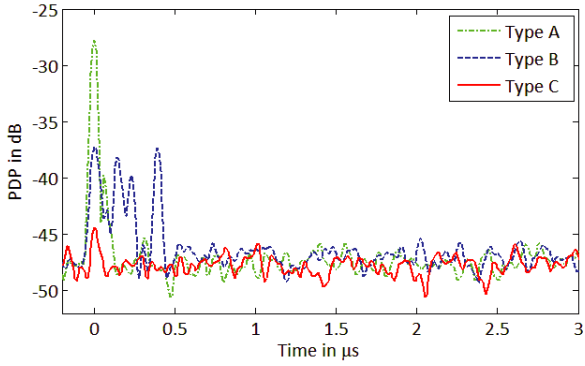

Figure 4. Examples of the measured PDPs with the transmitter at 400–500 m behind a Type A ship, a Type B ship, and a Type C ship.

the differences between the NLoS scenarios caused by different ship types, power delay profile (PDP) which is proportional to $|\hat{h}(t,\tau)|^2$ is used. The measured PDPs for propagations at a distance of around 400–500 m behind each type of ship are shown in Fig. 4 respectively. It is noted that the presented PDP is an average of 20 frames of instantaneous profile (around 0.2 ms) in this study while the system gain and the processing gain for PN sequence are not removed. From Fig. 4, it can be observed that the Type B ships are the only type of ship that results in significant multipath components. These multipath components are from the diffractions caused by the complex top structures (tower-like structure) of a Type B ship as shown in Fig. 3(c).

To compare the measured propagation channels with the simulated ones, both the measured and simulated PDPs are compared and analyzed. In the following, the shadowing/diffraction from a Type B ship is presented due to the obvious multipath components caused by its more complex periodic top structures. One example of the measured and simulated PDPs is shown in Fig. 5. The PDPs were taken when the mobile transmitter is about 320 m behind a Type B ship.

From Fig. 5, it is shown that the PDPs from the measurement and the simulation are qualitatively comparable. For other types of obstruction ships, comparable results are also observed between the measurements and the simulations. It is noted that the difference in the amplitude values between the measurement and the simulation results are likely due to the inaccuracies in conductivities, permittivity's, sea surface conditions and the rough dimensions of the simplified models

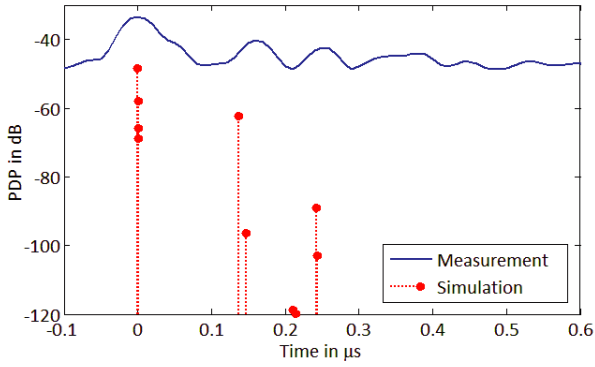

Figure 5. Comparisons of the measured and simulated PDPs with all multipath components.

(as shown in Fig. 3) created for the software simulation. This is expected since it is almost impossible to simulate the actual maritime environment and the obstruction ships. Similar conclusions have been reported in [25] when the Wireless InSite software is used to model an outdoor environment at 5 GHz and compared to their measurements.

Moreover, the measurement results indicate that two or more multipath clusters (A cluster is a combination of many multipath components which cannot be resolved by the channel sounding used.) are observed around 60% of the sea trial time when Type B ships act as an obstruction ship, while multipath components are observed only around 22% of the trial time for Type A ships. The percentage information (60% and 22%) is a summarization of the observed multipath propagations when the speed boat is in the planned zigzag route. It is noted that there is no multipath component observed in the PDPs for Type C ships. This is because the signal strength is extremely weak or falls into the noise floor when the mobile transmitter is behind the huge metallic body of a Type C ship since this type of ships are characterized by its high height above the sea level.

4. STAND-OFF DISTANCES

From the above studies, it is found that the diffractions from the ship's top structures and the shadowing due to its huge metallic body are the two main propagation mechanisms for the NLoS maritime applications. When the metallic body of a cargo ship is in middle of a propagation path, the communication link between the mobile transmitter and the control station could be lost or even fully blocked with a fixed transmitted power (e.g., 30 dBm in our measurements). The unavailability of the microwave link could be disastrous for certain applications, such as the control of an USV.

To characterize this phenomenon and provide some useful information for maritime microwave surveillance (e.g., a safe distance off an obstruction ship for establishment of a reliable communication link), the parameter *stand-off distance* d_{so} is adopted. In this work, it is determined at the first local maximum point of the SNR value (larger than 10 dB) as the distance behind the obstruction ship increases.

4.1. Tracing the Signal with Transmitter Position

In order to estimate the stand-off distance for the NLoS maritime applications obstructed by a cargo ship, the SNR was traced against the position of a mobile transmitter. Fig. 6 shows an example of the scatter plot for the SNR in dB versus the transmitter position. The

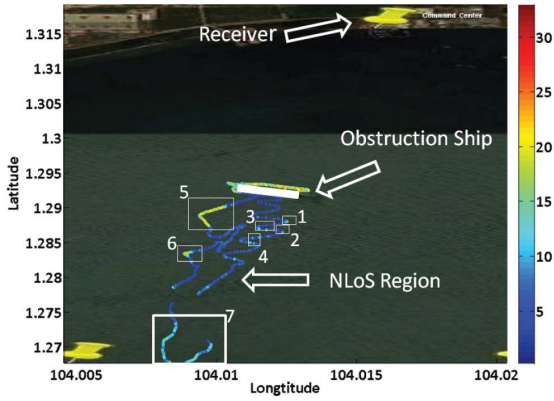

Figure 6. Example of SNR scatter plot in dB versus the transmitter position.

SNR shown in Fig. 6 is after correlating the known transmitted signal with the received signal [7, 18, 22]. Our observations indicate that when the transmitter boat is right behind (5–10 m away from) an obstruction ship, the received SNR is small (< 10 dB). This is true for all types of ships. This is because the transmitter boat has a relatively small size compared to the cargo ships and therefore, the transmitted signal is almost fully blocked. When the transmitter boat moves away from the cargo ship, the received SNR increases (as indicated in zone 1, 2, 3 and 4 of Fig. 6). The amount of increment in SNR depends on the amount of diffraction from the top structures of an obstruction ship. When the transmitter boat goes further beyond 1.2 km (shown in zone 7 of Fig. 6), the mobile transmitter is far away from the obstruction ship and therefore, the communication link approaches a LoS condition. A good communication channel can then be established again. However, due to the long distance, the SNR is weak. It is noted that, there is relatively high SNR shown in zone 5 and 6 of Fig. 6 due to the LoS transmission as the mobile transmitter goes beyond the shadowed areas of the obstruction ship.

Both the measurement and simulation results were then used to evaluate the stand-off distances for different types of obstruction ships. A summary of the evaluated stand-off distance together with the ship dimensions and the distance of the obstruction ship off the shore are tabulated in Table 1. From the results, it can be observed that there is no stand-off distance for Type C ships. This is because the Type C ship has the highest metallic body above the sea level among all the types of ships, and therefore, the communication link is almost fully

Table 1. Summary of ship information and stand-off distances.

Ships	Type A			Type B			Type C
	A1	A2	A3	B1	B2	B3	C1
Length	225 m	289 m	229 m	186 m	190 m	199 m	199 m
Width	32 m	45 m	38 m	30 m	32 m	34 m	32 m
Height	9.5 m	18.7 m	13.9 m	8.75 m	11 m	10 m	32.3 m
d_{s2s}	2.65 km	3.73 km	4 km	2.83 km	3 km	2.6 km	4.13 km
Stand-off distance d_{so}							
Measured	470 m	750 m	610 m	350–400 m	300 m	380 m	–
Simulated	510 m	760 m	550 m	400 m	320 m	430 m	–
Modelled	546 m	1200 m	644 m	400 m (R)	306 m	471 m	–

Notes: Height is the ship height above sea level, and d_{s2s} is the ship-to-shore distance. Ship A1 is *An Ho*, A2 is *Ban Ai Hai*, and A3 is *Welhero*; Ship B1 is *Elena*, B2 is *Favorita*, and B3 is *Thalassini*; and Ship C1 is *Grand Hero*.

blocked for the specific measurement campaign and could make the stand-off distance bigger than the transmission range of consideration. It is also found that the estimated stand-off distance is dependent on the size of an obstruction ship. Moreover, conclusions for Type B and Type A ships are varied. Normally, the stand-off distance is shorter for Type B ships as compared to Type A ships. This could be due to the tower-like structures of a Type B ship which may be suitable for knife-edge diffractions. The effect of knife-edge diffraction on the estimated stand-off distance is discussed below.

4.2. Influence from Knife-edge Diffraction

The tower-like structure of a Type B ship is first modeled as an ideal obstacle as shown in Fig. 7. The knife-edge diffraction model indicates that the diffraction gain is related to the Fresnel diffraction parameter v [24] which depends on the effective height h of an obstruction ship, the signal wavelength λ, the distance d_1 between the transmitter and the obstruction ship and the distance d_2 between the receiver and the obstruction ship as illustrated in Fig. 7. Since the distance between the transmitter and the receiver is relatively larger (> 2000 m) compared to the receiver height h_r of 10 m, the angel θ is small (of the order 10^{-5} degree). The effective height h of the obstruction ship is therefore approximately the difference between the height of the obstruction ship above the sea surface and the height h_t of the transmitter.

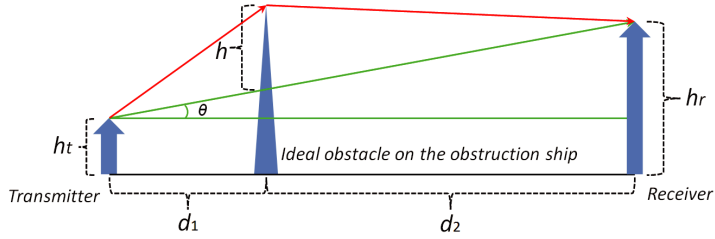

Figure 7. The geometry for knife-edge diffraction on an ideal obstacle.

It is noted that larger knife-edge diffraction loss L_{kf} can be introduced by a higher value of v which is proportional to the effective height h of an obstruction ship. Therefore, the higher the ship body is above the sea level, the longer the stand-off distance due to the larger diffraction loss. The observations in our sea trials have validated this point when studying a single type of ship. However, when comparing the results between Type A and Type B obstruction ships, the accuracy of the knife-edge diffraction model seems lost. From the ray tracing simulations, it was identified that the knife-edge diffraction for Type B ship is from its periodic top structures. Therefore, a height of 10–20 m of the structure should be added to the effective height h of a Type B ship if the knife-edge diffraction model is used. This would result in a generally higher effective height for Type B ships than that for Type A ships. However, it is observed in Table 1 that the stand-off distance for Type B obstruction ship is normally shorter compared to the stand-off distance for Type A ship. This may be because the knife-edge diffraction model for an ideal obstacle could only be applied to Type B ships since the periodic top structures of Type B ships have sharp edges (knife-edge).

The relatively flat/round body of Type A ships may decrease the accuracy of the knife-edge diffraction model. To properly evaluate the diffraction effect, Type A ship is then modelled as a rounded obstacle. The geometry of diffraction for this type of ship is illustrated in Fig. 8. For this diffraction scenario, an excess loss L_{ex} is added to the knife-edge diffraction loss L_{kf}. The excess loss L_{ex} is given as [14]:

$$L_{ex} \cong 11.7 \left\{ \frac{\pi r}{\lambda} \right\}^{\frac{1}{3}} \alpha \tag{2}$$

where r and α are shown in Fig. 8. Taking into consideration the excess loss, although the effective height h of Type A ship is shorter than that of Type B ship, the stand-off distance for Type A ship is generally longer than the stand-off distance for Type B ship due to its higher resultant loss of $(L_{kf} + L_{ex})$.

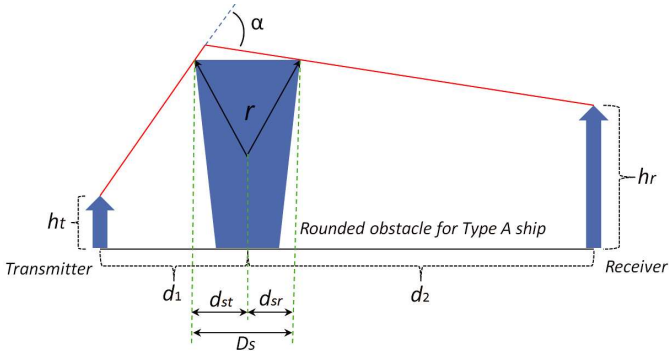

Figure 8. The geometry for knife-edge diffraction on a rounded obstacle.

Addition to the measured and simulated stand-off distances in Table 1, we also modelled/calculated the stand-off distances using the diffraction loss model where only the knife-edge diffraction L_{kf} is used for Type B ship and the resultant loss of the knife-edge diffraction L_{kf} with the excess loss L_{ex} is considered for Type A ship. Due to the imperfect sea surface conditions, neither the free-space model nor the 2-ray model could precisely predict the over-sea propagation loss. Therefore, a relative analysis is performed with a threshold for the maximum diffraction loss which is obtained using the Type B ship, 'Elena' in this study.

Based on the simulated stand-off distance for 'Elena', the diffraction loss threshold is determined. Using this diffraction loss as a threshold, the modelled stand-off distances for all the other obstruction ships are estimated and shown in the last row of Table 1. From Table 1, it is observed that the modelled stand-off distances are close to the measured and simulated stand-off values. Since the periodic top structure of Type B ships can be seen as an ideal knife-edge obstacle, the modelled values of stand-off distance for this type of ships are closer to the measured and simulated values. However, as the body of the Type A ships is not really a rounded obstacle, the modelled values of stand-off distance for Type A ships differs a lot from the measured and simulated values compared to the cases for Type B ships.

Generally, the main reason for the observed differences between the measured, simulated and modelled values of the stand-off distances in Table 1 is because, the simulation model using the ray tracing software is a simplified model and not an exact representation for the actual experiment scenario, while the modelled ones are estimated values and therefore differ from the measured ones. Moreover, other

environmental effects like sea surface conditions are also not taken into consideration for both the simulated and modelled results.

5. CONCLUSION

In this paper, we presented an investigation of the NLoS maritime mobile radio channels in 5 GHz band. Different types of cargo ships were examined as an obstruction to form NLoS maritime propagations. 3-D ray tracing has been used to assist the understanding of such an NLoS scenario. Theoretical models have also been used to verify the experimental results. Besides the PDPs, the stand-off distance is introduced in this study to analyze the NLoS propagations for surveillance applications. The measured PDPs and the stand-off distances are found to be comparable qualitatively with the simulated and modelled results.

The simulation results show that, rich multipath propagations can be observed for Type B ships due to the diffractions from their periodic top structures. The multipaths from these structures result in a shorter stand-off distance for Type B ships compared to Type A and Type C ships. These structures could be considered as ideal obstacles for knife-edge diffraction and can be properly modelled using the knife-edge diffraction model. For Type A ships, the simulation results agree well with the measured results with introducing an excess loss for their near-round structures. Taking into consideration this excess loss, the measured, simulated and modelled stand-off distances are also comparable. Furthermore, the huge metallic body of a Type C ship could fully block the microwave link, and therefore other communication solutions such as a satellite link are suggested.

Finally, it is noted that the geometries to model an realistic ship could be more complicated than the simplified model currently used for verifications of the measurement results in this study [16], and could be an interesting research topic in ray tracing.

ACKNOWLEDGMENT

This work was supported in part by the Defence Science and Technology Agency (DSTA), Singapore.

REFERENCES

1. Inoue, T. and T. Akiyama, "Propagation characteristics on line-of-sight over-sea paths in Japan," *IEEE Trans. Antennas Propag.*, Vol. 22, No. 4, 557–565, 1974.

2. Hitney, H. V. and L. R. Hitney, "Frequency diversity effects of evaporation duct propagation," *IEEE Trans. Antennas Propag.*, Vol. 38, No. 10, 1694–1700, 1990.
3. Maliatsos, K., P. Constantinou, P. Dallas, et al., "Measuring and modeling the wideband mobile channel for above the sea propagation paths," *European Conf. Antennas Propag.*, Nice, France, 2006.
4. Yang, K., T. Roste, F. Bekkadal, et al., "Long-distance propagation measurements of mobile radio channel over sea at 2 GHz," *2011 IEEE Veh. Technol Conf.*, San Francisco, CA, 2011.
5. Timmins, I. J. and S. O'Young, "Marine communications channel modeling using the finite-difference time domain method," *IEEE Trans. Veh. Technol.*, Vol. 58, No. 6, 2626–2637, 2009.
6. Lei, Q. and M. Rice, "Multipath channel model for over-water aeronautical telemetry," *IEEE Trans. Aerosp. Electron. Syst.*, Vol. 45, No. 2, 735–742, 2009.
7. Meng, Y. S. and Y. H. Lee, "Measurements and characterizations of air-to-ground channel over sea surface at C-band with low airborne altitudes," *IEEE Trans. Veh. Technol.*, Vol. 60, No. 4, 1943–1948, 2011.
8. Lee, Y. H. and Y. S. Meng, "Empirical modeling of ducting effects on a mobile microwave link over a sea surface," *Radioengineering*, Vol. 21, No. 4, 1054–1059, 2012.
9. Joe, J., S. K. Hazra, S. H. Toh, et al., "Path loss measurements in sea port for WiMAX," *IEEE Wirel. Commun. Netw. Conf.*, Kowloon, 2007.
10. Hu, C. F., Z. Zhou, and S. X. Guo, "A synchronous wideband frequency-domain method for long-distance channel measurement," *Progress In Electromagnetics Research*, Vol. 137, 643–652, 2013.
11. Matolak, D. W., I. Sen, and W. Xiong, "The 5-GHz airport surface area channel — Part I: Measurement and modeling results for large airports," *IEEE Trans. Veh. Technol.*, Vol. 57, No. 4, 2014–2026, 2008.
12. Sen, I. and D. W. Matolak, "The 5-GHz airport surface area channel — Part II: Measurement and modeling results for small airports," *IEEE Trans. Veh. Technol.*, Vol. 57, No. 4, 2027–2035, 2008.
13. Dong, F., C. W. Chan, and Y. H. Lee, "Channel modeling in maritime environment for USV," *Defence Technol. Asia 2011*, Singapore, 2011.

14. Parsons, J. D., *The Mobile Radio Propagation Channel*, 2nd Edition, Wiley, New York, 2000.
15. Durgin, G., T. S. Rappaport, and H. Xu, "Measurements and models for radio path loss and penetration loss in and around homes and trees at 5.85 GHz," *IEEE Trans. Commun.*, Vol. 46, No. 11, 1484–1496, 1998.
16. Bertoni, H. L., *Radio Propagation for Modern Wireless Systems*, Prentice Hall PTR, New Jersey, 2000.
17. Meng, Y. S., Y. H. Lee, and B. C. Ng, "The effects of tropical weather on radio wave propagation over foliage channel," *IEEE Trans. Veh. Technol.*, Vol. 58, No. 8, 4023–4030, 2009.
18. Meng, Y. S., Y. H. Lee, and B. C. Ng, "Further study of rainfall effect on VHF forested radio-wave propagation with four-layered model," *Progress In Electromagnetics Research*, Vol. 99, 149–161, 2009.
19. FEMA 426, *Reference Manual to Mitigate Potential Terrorist Attacks Against Buildings*, Risk Management Series, Federal Emergency Management Agency, 2003.
20. Dong, F. and Y. H. Lee, "Non-line-of-sight communication links over sea surface at 5.5 GHz," *2011 Asia-Pacific Microw. Conf.*, Melbourne, VIC, 2011.
21. Dong, F. and Y. H. Lee, "Experiment results of a two-by-two diverse antennas system over the sea surface in NLOS scenario," *IEEE APS Int. Symp. Antennas Propag.*, Chicago, USA, 2012.
22. Meng, Y. S. and Y. H. Lee, "Practical wideband channel sounding system for air-to-ground measurements at C band," *IEEE Int. Instrum. Meas. Technol. Conf.*, Singapore, 2009.
23. Wireless InSite, Version 2.2, Remcom Inc., State College, PA, 2006, www.remcom.com.
24. Rappaport, T. S., *Wireless Communications Principles and Practice*, Prentice-Hall Inc., NJ, 2002.
25. Davis, N., "Comparison of ray tracing and measurement results for 5 GHz band wireless channels," M.Sc. Thesis, Ohio University, 2009.